The Conformation of B18 Peptide in the Presence of Fluorinated and Alkylated Nanoparticles

Sandra Rocha,[a, c] Andreas F. Thünemann,*[b] M. Carmo Pereira,[c] Manuel A. N. Coelho,[c] Helmuth Möhwald,[a] and Gerald Brezesinski[a]

The misfolding and aggregation of proteins into amyloid fibrils are thought to be the cause of various neurological and systemic diseases.[1] Amyloid fibrils consist of polypeptide chains organized into β-sheets.[2] In contrast, the secondary structure of the native proteins is dominated by α-helical and random-coil conformations. Therefore, the inhibition of conformational transitions and subsequent fibril formation constitute a possible approach for preventing the progression of amyloid-related diseases.

Peptides consisting of short sequences with twelve to twenty residues have been shown to self assemble into fibrils with ultrastructures similar to those of larger polypeptides.[3] Hence these short sequences constitute ideal model systems for studying conformational changes and fibrillization in vitro.

This work focuses on changes in the secondary structure of the B18 peptide (LGLLLRHLRHHSNLLANI) when in contact with fluorinated and alkylated nanoparticles. B18 represents a segment (amino acids 103–120) of the protein bindin, found in *Strongylocentrotus purpuratus* (purple sea urchin). Bindin plays a key role in the fertilization process and the B18 sequence is recognized as the minimal membrane-binding and fusogenic motif.[4] B18 is a short peptide sequence with a strong tendency to self assemble and form amyloid fibrils.[5]

Structural studies of B18 peptide upon binding to lipid membranes revealed an oligomeric β-sheet structure, but an α-helical structure in lipid bilayers was also recently shown by NMR studies.[6] Fusogenic properties are believed to contribute to the neurotoxicity of amyloidogenic peptides by destabilizing cellular membranes and have been described for sequences of prion peptides and amyloid β-peptides.[7]

Fluorinated alcohols, such as trifluoroethanol, induce α-helical conformation in fibril-forming peptides.[8] This effect, however, is not observed with their alkylated analogues. Fluorinated alcohols are not biocompatible and therefore have no therapeutic relevance in vivo. However, polyelectrolyte–fluorosurfactant complexes can, in principle, be engineered with bio-

[a] *S. Rocha, Prof. Dr. H. Möhwald, Dr. G. Brezesinski*
Max Planck Institute of Colloids and Interfaces
Am Mühlenberg 1, 14476 Golm/Potsdam (Germany)

[b] *Dr. A. F. Thünemann*
Federal Institute for Materials Research and Testing
Richard-Willstätter-Straße 11, 12489 Berlin (Germany)
Fax: (+49) 308-104-1137
E-mail: andreas.thuenemann@bam.de

[c] *S. Rocha, Prof. M. C. Pereira, Prof. M. A. N. Coelho*
Faculty of Engineering, University of Porto
Rua Dr. Roberto Frias, 4200-465 Porto (Portugal)

  DOI: 10.1002/cbic.200400177

compatible properties.[9] It was previously demonstrated that these complexes are able to dissolve amyloid plaques in sections of animal tissue[9] and to convert β-sheet into α-helix structures.[10] These complexes were tested on solid supports in a first approach.

In order to increase the contact area between peptide molecules and complexes, polyampholytes with alternating cationic (*N,N′*-diallyl-*N,N′*-dimethylammonium chloride) and anionic charged monomers (*N*-phenylmaleamic acid) were synthesized with a degree of polymerization in the 60–80 units range (see Scheme 1). Polyampholytes and dodecanoic and perfluorododecanoic acid complexes were prepared. The result, in both cases, was nanoparticles with hydrodynamic diameters of about 4 nm (so-called polyampholyte dressed micelles).[11]

The radii of the nanoparticles were determined by small-angle X-ray scattering (HASYLAB at DESY, Hamburg, Germany). Dispersions of particles in water were transferred into glass capillaries that had a diameter of 1 mm. The intensity measured was corrected by using the intensity from a capillary filled with pure water.

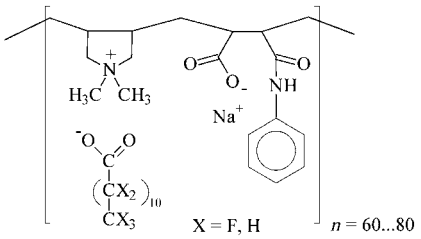

Scheme 1. *Complexes of poly(*N,N′*-diallyl*-N,N′*-dimethylammonium*-alt-N-*phenyl-maleamic carboxylate) and the sodium salt of dodecanoic acid (X = H) and perfluorododecanoic acid (X = F).*[11]

The fluorinated nanoparticles produce a strong scattering intensity (see Figure 1 a) while the intensity of the alkylated nanoparticles is low (not shown). This difference can be explained by the different densities of the nanoparticles, which are 1.273 g cm^{-3} (alkylated) and 1.754 g cm^{-3} (fluorinated).[11] Taking into account that the small-angle scattering intensity is proportional to the square of the electron density difference between the particles and their surroundings (water), the scattering intensity of the fluorinated particles is expected to be one order of magnitude higher than that of their alkylated analogues. On the basis of the present data, we can therefore only evaluate the scattering of the fluorinated nanoparticles. The scattering vector is defined as $s = (2/\lambda)\sin\theta$, where θ is the scattering angle and λ is the wavelength. It can be seen in Figure 1 that the scattering intensity decreases proportionally to s^{-4} at high values of s; this is a Porod asymptote.

Sharp phase boundaries are identified by the presence of Porod's law[12] which is given by:

$$\lim_{s\to\infty} 2\pi^3 s^4 I(s) = \frac{k}{l_p} \qquad (1)$$

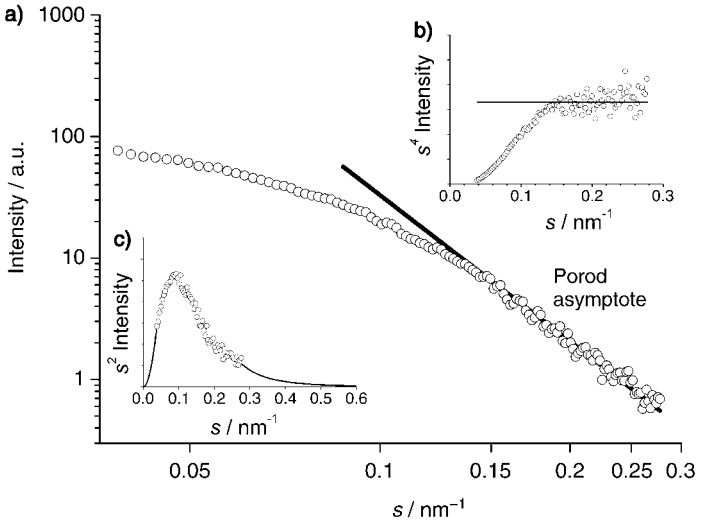

Figure 1. *a) Small-angle X-ray scattering intensity of fluorinated nanoparticles (○). The straight line indicates the Porod asymptote. The scattering vector is defined as* $s = (2/\lambda)\sin\theta$. *The* $s^4 I(s) - s$ *plot in insert. b)* $s^4 I(s) - s$ *plot showing the asymptotic behaviour of the data (○). The solid line represents the best fit according to Porod's law performed in the 0.15–0.28 nm*$^{-1}$ *range. The area under the curve is in c). c) Represents the invariant* k. *Experimental values (○) are only available between a lower limiting value of the scattering vector* s_{min} *and an upper value* s_{max}. *Extrapolations (solid lines) below* s_{min} *and above* s_{max} *were carried out to calculate the invariant as precisely as possible. The cord length of the fluorinated nanoparticles is 2.7 nm, and the radius is 2.0 nm.*

where I is the scattering intensity, l_p is the average cord length and k is the invariant given by the expression:

$$k = 4\pi \int_0^\infty s^2 I(s)\,ds \qquad (2)$$

The scattering intensity is experimentally obtained from a range lying between a lower limiting value of the scattering vector s_{min} and an upper value s_{max}. In order to calculate the invariant as precisely as possible, the experimental limits were taken into account by approximation of the region of high and low scattering vectors, resulting in:

$$k = {}^4\!/_3\pi s_{min}^3 I(s_{min}) + 4\pi \int_{s_{min}}^{s_{max}} s^2 I(s)\,ds + \frac{4\pi}{s_{max}} \lim_{s\to\infty} [s^4 I(s)] \qquad (3)$$

A similar approximation for measurements performed with a Kratky camera was earlier used by Ruland.[13] We have previously used Equation (3) to determine k precisely for poly(ethylene imine)–retinoic acid complexes.[14]

The areas under the solid lines in Figure 1 c correspond to the first and third term in Equation (3) and add up to 30% of the invariant, which cannot be neglected. The main source of error in the range of validity covered by Porod's law is the scattering due to density fluctuations and the widths of the domain boundary.[15] The value of $s^4 I(s)$, as shown in Figure 1 b, was found to be constant for a scattering vector in the range of 0.15 to 0.28 nm^{-1}. This proves that the structures of the nanoparticles are consistent with Porod's law. A broader transition or a statistical structuring of the domain boundary, as typi-

cally observed in microphase-separated block copolymers in bulk materials,[16] can be excluded. Small deviations from a sharp boundary would indicate a significant deviation from Porod's law.[15] Therefore, we can conclude that the phase boundaries of the nanoparticles are of the order of one to two atomic distances. By using Equation (1), the average chord length was calculated to be 2.7 nm. The radius of a spherical particle[17] is then given by $r = {}^3/_4 l_p$, which is 2.0 nm. This value for the radius is in agreement with the values determined by analytical ultracentrifugation and dynamic light-scattering measurements.[11]

The nanoparticles display negative surface charges with zeta potentials in the range of -20 to -50 mV and dissolve at concentrations lower than 0.02 g L^{-1} (this indicates that they are not covalently cross-linked). Due to their small size they have specific surface areas of approximately 1000 m^2 g^{-1}. The high surface area can be expected to be useful in providing extensive interactions with the peptide. The nanoparticles consist of a hydrophobic core (formed by the surfactant chains) and a hydrophilic shell. Here the low-molecular-weight counter ions (Na^+) of the micelle are replaced by the polyampholyte.

The aim of this study is to compare the influence of the fluorinated and hydrogenated nanoparticles on the secondary structure of B18. The investigations were performed at two distinct pH values: pH 4, at which B18 has five positive charges (the side chains of three histidines and two arginines are protonated), and pH 7, at which approximately 10% of the peptide has two protonated arginines and forms fibrils.[5] Assuming a pK_a of 6.3 for each of the three His residues, then, at pH 7, the B18 peptide coexists as a dynamic mixture of differently protonated peptides: with all three His residues unprotonated (51%), with one His protonated (38%), with two His residues protonated (10%), and with all three His residues protonated (1%). The three His residues are probably not independent, and one might expect some changes in their pK_a's due to neighbouring effects.

Circular dichroism (CD) measurements were performed to determine the secondary structure of the B18 peptide after titration with different amounts of nanoparticles. Final particle concentrations were 0, 2, 4 and 6 g L^{-1} at a temperature of 20 ± 1 °C. The corresponding molar concentrations of the particles are in the range of about $6–18 \times 10^{-5}$ mol L^{-1}, which is close to the molar concentration of B18 (10×10^{-5} mol L^{-1}).

The measured CD spectra are shown in Figures 2 (pH 4) and 3 (pH 7). It can be seen from these figures (curves 1) that, in the absence of particles, B18 displays the typical spectrum of a random-coil protein (minimum at 198 nm). For a quantitative determination of the secondary structure, the content of structural motifs was calculated according to Greenfield.[18] This results in a content of 4% α-helix, 18% β-sheet and 78% random coil at pH 4 without contact to nanoparticles. At pH 7, the values were 2% α-helix, 24% β-sheet and 74% random coil.

The titration of B18 with increasing amounts of fluorinated nanoparticles at pH 4 induces a change from random coil to α-helix structure, as shown in Figure 2a (curves 2–4). The α-helix content was found to be 22%, 38% and 44% for 2, 4, and 6 g L^{-1} fluorinated nanoparticles, respectively. An isosbestic point can be seen at 203 nm (Figure 2a); this indicates an equilibrium between two conformational states. The dominating process is the transformation of random coil to α-helix, which is responsible for the observation of the isosbestic point. The small fraction of β-sheet present at pH 4 remains mainly unchanged. Our finding is in line with results reported earlier by Glaser et al.,[19] who showed that the titration of B18 with increasing amounts of trifluoroethanol also induced a change from random coil to α-helix.

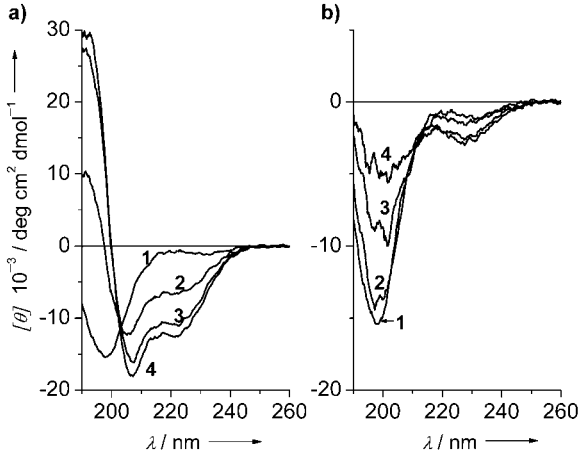

Figure 2. CD data of B18 (96 μM in acetate buffer) at pH 4 in the presence of a) fluorinated and b) alkylated nanoparticles at 0 g L^{-1} (curve 1), 2 g L^{-1} (curve 2), 4 g L^{-1} (curve 3) and 6 g L^{-1} (curve 4). The curves are normalized by peptide concentration and cell path length.

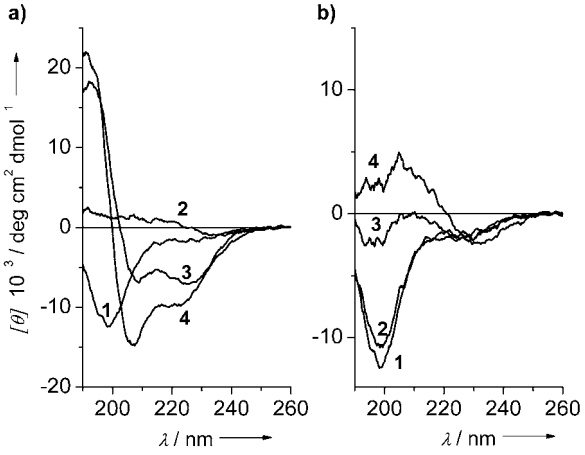

Figure 3. CD data of B18 (96 μM in phosphate buffer) at pH 7 in the presence of a) fluorinated and b) alkylated nanoparticles at 0 g L^{-1} (curve 1), 2 g L^{-1} (curve 2), 4 g L^{-1} (curve 3) and 6 g L^{-1} (curve 4). The curves are normalized by peptide concentration and cell path length.

The alkylated particles, in contrast to the fluorinated nanoparticles, do not induce α-helix-rich structures at pH 4 (Figure 2b). Titration of B18 with alkylated nanoparticles resulted in a decrease in the CD signal with increasing concentration of the nanoparticles (Figure 2b, curves 2–4). This was accompanied by the occurrence of turbidity in the solution. The presence of an isosbestic point at 210 nm indicates a two-state transition from random coil to a β-sheet-rich structure. This suggests that β-sheet structures are present in B18 for the

higher particle concentrations (4 and 6 g L^{-1}), but, due to the strong light scattering of the B18 aggregates, the distribution of structure motifs could not be calculated. A possible reason for the occurrence of aggregates in the case of alkylated particles might be charge compensation between the negatively charged nanoparticles and the positively charged B18.

The changes in the secondary structure of B18 at pH 7 are shown in Figure 3. Again a transition from random-coil to α-helix structure after titration with the fluorinated nanoparticles is observed, but the behaviour is more complex. The CD-signal intensity (Figure 3a, curve 2) is close to zero at small nanoparticle concentrations (2 g L^{-1}), and a high turbidity in the solution is observed. This is probably due to charge neutralization between B18 and the particles.

At higher nanoparticle concentrations, the solutions are transparent, and the shapes of the CD curves are typical for α-helix structures. The content of α-helix was estimated to be 14% or 34% for particle concentrations of 4 g L^{-1} and 6 g L^{-1}, respectively. A further increase in the nanoparticle concentration does not result in a higher α-helix content.

Binder et al.[20] reported that Zn^{2+} ions induce α-helix structure in B18 by specific complexation with the histidine-rich sequence of B18 (HxxHH). In the absence of Zn^{2+}, the peptide is rapidly inactivated at pH 7 or higher, by aggregation into β-sheet amyloid fibrils. The fluorinated particles at a suitably high concentration seem to have a similar effect on B18 as Zn^{2+} or α-helix-inducing solvents (trifluoroethanol).

For alkylated nanoparticles at pH 7, the change of the CD signal is low at a particle concentration of 2 g L^{-1} but changes greatly at the higher concentrations (see Figure 3b). This was accompanied by significant precipitation. A calculation of the percentages of the different secondary structures was therefore not possible. Nevertheless, from the shape of the spectra (curves 3 and 4 in Figure 3b) B18 seems to mainly contain β-sheet and random-coil motifs at particle concentrations of 4 and 6 g L^{-1}.

Negatively charged fluorinated nanoparticles induce α-helix structures in the B18 peptide at pH 4 and 7, whereas the negatively charged alkylated ones lead to aggregation or β-sheet formation. These results reinforce the idea that electrostatic interactions are not the major force in determining the helical state of the peptide. It is likely that B18 interacts with nanoparticles by hydrophobic interactions, which are enhanced in the case of fluorinated nanoparticles due to the presence of perfluorinated alkyl chains. This might explain why fluorinated particles but not alkylated ones induce α-helix-rich structures in B18. Since the degree of helicity in the presence of fluorinated particles is higher at pH 4, both electrostatic and hydrophobic interactions seem to be responsible for stabilizing the helical structures.

The strong effect of fluorinated nanoparticles indicates that a dynamic structure in which part of the fluorinated chains is in contact with the hydrophilic phase. This suggests that proper micelle engineering is required for optimum response. This means: i) enough fluorinated alkyl chains in the hydrophilic phase to affect the peptide, ii) a suitable particle/peptide ratio to avoid precipitation.

In conclusion, it has been demonstrated that fluorinated nanoparticles made of a polyampholyte–fluorosurfactant complex induce α-helix-rich structure in B18 at both pH 4 and 7, whereas their alkylated analogues do not have this effect. Fluorinated nanoparticles are proposed to be potential candidates for the inhibition and reversion of conformational changes of proteins that lead to amyloid fibril formation.

Acknowledgements

These investigations were supported by the Max Planck Society, the Fraunhofer Society, the Deutsche Forschungsgemeinschaft (BR1378/8-2) and the Federal Institute of Material Research and Testing. S.R. thanks the Fundação para a Ciência e a Tecnologia for a Fellowship (BD/948/2000). O. Zschörnig from the University of Leipzig is acknowledged for providing the B18 peptide. SAXS measurements were performed at HASYLAB beam line A2 at DESY, Hamburg, Germany.

Keywords: B18 peptide · circular dichroism · conformational analysis · fluorine · nanostructures

[1] D. J. Selkoe, *Nature* **2003**, *426*, 900–904.
[2] M. Sunde, C. Blake, *Adv. Protein Chem.* **1997**, *50*, 123–159.
[3] a) K. Halverson, P. E. Fraser, D. A. Kirschner, P. T. Lansbury Jr, *Biochemistry* **1990**, *29*, 2639–2644; b) C. J. Barrow, M. G. Zagorski, *Science* **1991**, *253*, 179–182.
[4] A. Hofmann, C. G. Glabe, *Semin. Dev. Biol.* **1994**, *5*, 233–242.
[5] A. S. Ulrich, W. Tichelaar, G. Förster, O. Zschörnig, S. Weinkauf, H. W. Meyer, *Biophys. J.* **1999**, *77*, 829–841.
[6] a) P. Barré, O. Zschörnig, K. Arnold, D. Huster, *Biochemistry* **2003**, *42*, 8377–8386. S; b) S. Afonin, U. H. N. Dürr, R. W. Glaser, A. S. Ulrich, *Magn. Reson. Chem.* **2004**, *42*, 195–203.
[7] a) T. Pillot, M. Goethals, B. Vanloo, C. Talussot, R. Brasseur, J. Vandekerckhove, M. Rosseneu, L. Lins, *J. Biol. Chem.* **1996**, *271*, 28757–28765; b) T. Pillot, L. Lins, M. Goethals, B. Vanloo, J. Baert, J. Vandekerckhove, M. Rosseneu, R. Brasseur, *J. Mol. Biol.* **1997**, *274*, 381–393.
[8] a) C. J. Barrow, A. Yasuda, P. T. M. Kenny, M. G. Zagorski, *J. Mol. Biol.* **1992**, *225*, 1075–1093; b) H. Zhang, K. Kaneko, J. T. Nguyen, T. L. Livshits, M. A. Baldwin, F. E. Cohen, T. L. James, S. B. Prusiner, *J. Mol. Biol.* **1995**, *250*, 514–526.
[9] A. F. Thünemann, E. P. Vieira, H. Hermel, H. Motschmann, H. Möhwald, W. Schmahl, K. Matiasek, C. Sperling, C. Werner (Max Planck Society), European Patent application EP1341564.
[10] E. P. Vieira, H. Hermel, H. Möhwald, *Biochim. Biophys. Acta* **2003**, *1645*, 6–14.
[11] A. F. Thünemann, K. Sander, W. Jaeger, R. Dimova, *Langmuir* **2002**, *18*, 5099–5105.
[12] M. A. Micha, C. Burger, M. Antonietti, *Macromolecules* **1998**, *31*, 5930–5933.
[13] N. Stribeck, W. Ruland, *J. Appl. Crystallogr.* **1978**, *11*, 535–539.
[14] A. F. Thünemann, J. Beyermann, *Macromolecules* **2000**, *33*, 6878–6885.
[15] U. Siemann, W. Ruland, *Colloid Polym. Sci.* **1982**, *260*, 999–1010.
[16] T. Wolff, C. Burger, W. Ruland, *Macromolecules* **1994**, *27*, 3301–3309.
[17] C. Burger, W. Ruland, *Acta Crystallogr.* **2001**, *A57*, 482–491.
[18] N. Greenfield, G. D. Fasman, *Biochemistry* **1969**, *8*, 4108–4116.
[19] R. W. Glaser, M. Grüne, C. Wandelt, A. S. Ulrich, *Biochemistry* **1999**, *38*, 2560–2569.
[20] H. Binder, K. Arnold, A. S. Ulrich, O. Zschörnig, *Biochim. Biophys. Acta* **2000**, *1468*, 345–358.

Received: May 28, 2004
Published online: January 11, 2005

